EXPERIMENTAL ELECTRON CAPTURE CROSS SECTIONS IN COLLISIONS OF HIGHLY-CHARGED LOW-VELOCITY RARE GAS IONS WITH LITHIUM ATOMS

by

WILLIAM TRACY WAGGONER

B.A., Hastings College, 1980

A MASTER'S THESIS

submitted in partial fulfillment of the

requirements for the degree

MASTER OF SCIENCE

Department of Physics

KANSAS STATE UNIVERSITY
Manhattan, Kansas

1983

Approved by:

C L Coche
Major Professor

THIS BOOK
CONTAINS
NUMEROUS PAGES
WITH THE ORIGINAL
PRINTING BEING
SKEWED
DIFFERENTLY FROM
THE TOP OF THE
PAGE TO THE
BOTTOM.

THIS IS AS RECEIVED
FROM THE
CUSTOMER.

TABLE OF CONTENTS

LIST OF FIGURES

ACKNOWLEDGEMENTS

I would like to thank my family for their love and encouragement over the years. To them all my love.

I would like to thank Dr. C.L. Cocke for the counseling and patient guidance he provided during the execution of this work.

I would like to thank Dr. E. Justiniano for his friendship and for the many helpful discussions involving this work.

I would like to acknowledge Dr. S.L. Vargheese, Dr. M. Stoeckli, C. Can, C. Schmeissner, L. Tunnell and A. Skutlartz for their assistance in data acquisition, as well as for their friendship and support.

I wish to thank D. Claassen, P. Lewis, and the members of the MeV's for their friendship and support.

A final word of thanks to Sandy Chandler who typed this thesis, and to Walter Heimbaugh who did the drawings.

Finally, I acknowledge the U.S. Department of Energy, Division of Chemical Sciences for their financial support of this work.

Chapter 1

INTRODUCTION

In recent years the development of ion sources that could produce highly charged ions with velocities in the range of 10^6-10^7 cm/s has lead to the study of electron capture in low energy ion atom collisions. Such collisions involve the transfer of one or more electrons from a neutral target atom to a highly charged projectile ion moving slowly in comparison to the orbital velocities of the target electrons. Quantum mechanical descriptions of such collisions for systems more complex than bare nuclei colliding with one electron targets are rare. As a result many models based on simplifications of the problem have surfaced, and for this projectile velocity range require experimental results for comparison. The purpose of this work is to expand the pool of experimental data for such low-energy highly-charged (LEHQ) ion atom collisions, in order to aid the physical understanding of this range of collisions.

The interest in studying such systems is not only in the physics of the collision process, but also with the possible applications of the results. One possible application of interest is the development of lasers capable of lasing in the very high ultra-violet and soft x-ray spectral regions. Collision between neutral target atoms and multiply charged ions, where electrons are captured into excited states, has been proposed as a means to obtain population inversions capable of lasing in such regions.[1-3] Another area of interest in such collisions is that of controlled thermonuclear fusion research. Such collisions are important in

magnetically confined high temperature plasmas. The capture of a hydrogen electron into exited states of LEHQ impurity ions followed by radiation from the decaying excited states could lead to cooling of the plasma.[4,5] Another possible application is the use of the He^{2+} + Li collision system to monitor alpha particle distributions in the confined fusion plasmas.[6] One technique proposed is to monitor the radiation released when an excited He^{+} state, formed in such collisions, decays. Although the work presented here did not primarily involve the study of He^{2+} + Li collisions, some He^{2+} + Li data are presented in order to compare the present experimental results to data published in the literature.

This thesis specifically describes a study of electron capture from neutral Li target atoms by LEHQ rare gas ions (Ne, Ar, Kr, and Xe). Several motivations exist for studying these particular collision systems. Descriptions for collisions involving LEHQ ions are almost exclusively based on a one electron model for the target. Hence Li is a convenient choice for a target. In its ground state configuration, $1s^2$ 2s, the 2s Li electron is loosely bound with an ionization potential of 5.39 eV. Further the inner shell electrons are tightly bound, experimental results showing that single electron capture dominates the total electron capture cross section. Indeed the ionization potential of the neutral hydrogen atom is 13.6 eV, thus the Li 2s electron has a significantly lower binding energy and is more easily captured by LEHQ ions than the ground state hydrogen electron. Another feature of the theoretical model descriptions is that a structureless charged projectile is assumed. Thus these models neglet the structure of the projectile's electronic core. Experimental results for the LEHQ rare gas projectiles studied have indicated that the target electron is captured into high Rydberg states at large capture radii. For loosely bound Li

this n should be exceptionally high. Thus, the captured electron "sees" only a core charge and the treatment of the projectile as a point charge is expected to be better justified than for more tightly bound targets.

Presented in this thesis are the measured cross sections for electron capture from neutral Li atoms by LEHQ rare gas ions (Ne, Ar, Kr, and Xe). In Chapter 2 the experimental techniques used to collect data as well as the analytical methods used to calculate cross sections from this data are presented. Two theoretical models describing such collision processes are presented in Chapter 4 for comparison with the experimental results which are presented in Chapter 3. These results are discussed in relationship to those theories and arguments in Chapter 5. Finally, a summary of this work, as well as conclusions are presented in Chapter 6.

Chapter 2

EXPERIMENT

A. Experimental Configuration

(1) Production and detection of L.E.H.Q. Ions

The technique used to produce L.E.H.Q. ions for this experiment has previously been reported in the literature by Cocke[7], Gray, et al.[8] and Justiniano.[9] Fast pulsed 20 MeV F^{+4} and F^{+8} beams from the Kansas State University EN tanden Van de Graaff accelerator were passed through a gas cell containing rare gases to pruduce a source of ions. The fluorine beam was typically pulsed to a width of 5 ns or less at a repetition rate of 8 μsec. Figure 1 shows the scattering chamber experimental system which was kept at base pressures on the order of 2×10^{-6} torr. Ions created in the gas cell, called projectile ions, were extracted by applying voltages to the cell and the three-grid system contained within the cell. These ions then passed through a resistively heated Li vapor oven, and on into a double-focussing spherical sector electrostatic analyzer. The voltage, V_a, at which an ion is passed through the analyzer and onto detection is directly proportional to the ratio between the projectile ion's energy, and the charge state q' of the ion after passing through the oven. Since the energy of the projectile ion is determined by its initial charge state q, and the voltage it was extracted with V_1, the analyzer effectively measures the ratio between initial and final charge states, such that

$$V_a = K \frac{E}{q'} = K \frac{qV_1}{q'} \qquad (1)$$

THIS BOOK CONTAINS NUMEROUS PAGES THAT WERE BOUND WITHOUT PAGE NUMBERS.

THIS IS AS RECEIVED FROM CUSTOMER.

Figure 1: Schematic of experimental apparatus.

THIS BOOK CONTAINS NUMEROUS PAGES WITH DIAGRAMS THAT ARE CROOKED COMPARED TO THE REST OF THE INFORMATION ON THE PAGE.

THIS IS AS RECEIVED FROM CUSTOMER.

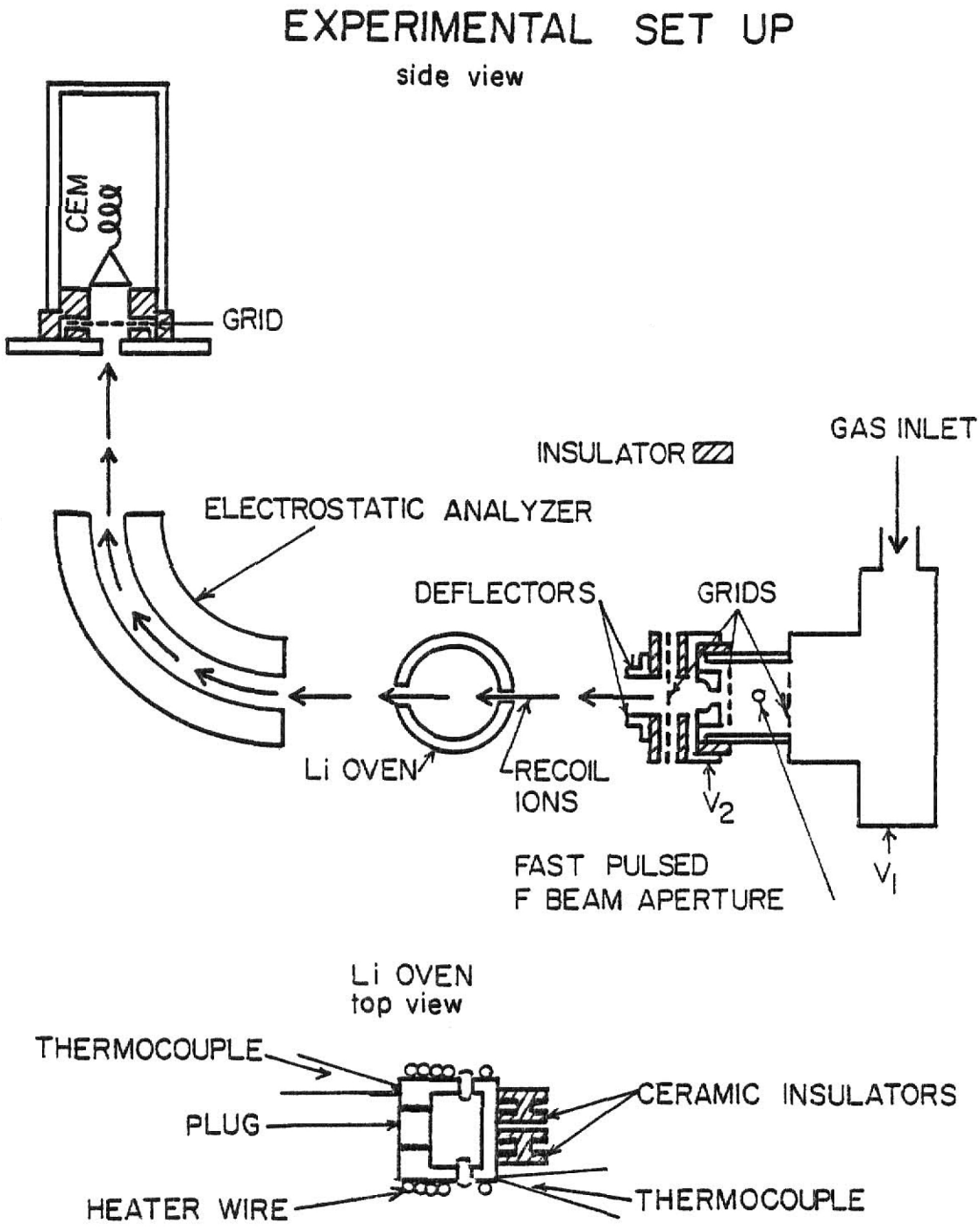
EXPERIMENTAL SET UP
side view
CEM
GRID
INSULATOR
GAS INLET
ELECTROSTATIC ANALYZER
DEFLECTORS
GRIDS
Li OVEN
RECOIL IONS
V_2
FAST PULSED F BEAM APERTURE
V_1
Li OVEN
top view
THERMOCOUPLE
PLUG
HEATER WIRE
CERAMIC INSULATORS
THERMOCOUPLE

FIGURE 1

where K is a constant depending on the geometry of the analyzer. The voltage applied to the analyzer was sweept from K V_1 to slightly above 2 K V_1 through the use of a triangle wave generator.

After passing through the analyzer, the projectile ions were detected with a channeltron as shown in Figure 1. The total time of flight of the ions from production to detection is proportional to $\sqrt{m/q}$. Upon detection the voltage, V_a, of the analyzer was sampled. The time of flight spectrum and the voltage spectrum are used to form a two-dimensional spectrum. A typical such spectrum is shown in Figure 2. From such spectrum we were then able to determine the initial charge state q, and the final charge state q' for any collision event. Events where projectile ions do not change charge state are analyzed at one voltage V_a = K V_1, and are called direct events. Events in which a single electron is captured lie on the curved line. A block diagram of the data gathering electronics is shown in Figure 3.

(2) Production of Li Vapor

A side view of the Li vapor oven is shown schematically in the lower half of Figure 1. The stainless steel cylindrical oven is 1.90 cm in diameter and 1.85 cm in length. The oven is attached to the mounting system of the analyzer by two ceramic standoffs on one end, and a tapped loading port is located on the other end. The oven is heated by passing a D.C. current through heater wire wrapped around the oven, and the current drawn and voltage applied were measured. Typical operating conditions were 1 amp of current drawn at an applied voltage of 15 volts. Two Chrommel-Alumel thermocouples were attached to opposite faces of the oven. Several methods were used to attach the thermocouples, the final method chosen being to silver solder the thermocouples directly to the

Figure 2: Two-dimensional spectrum for Ar^{q+} on Li.

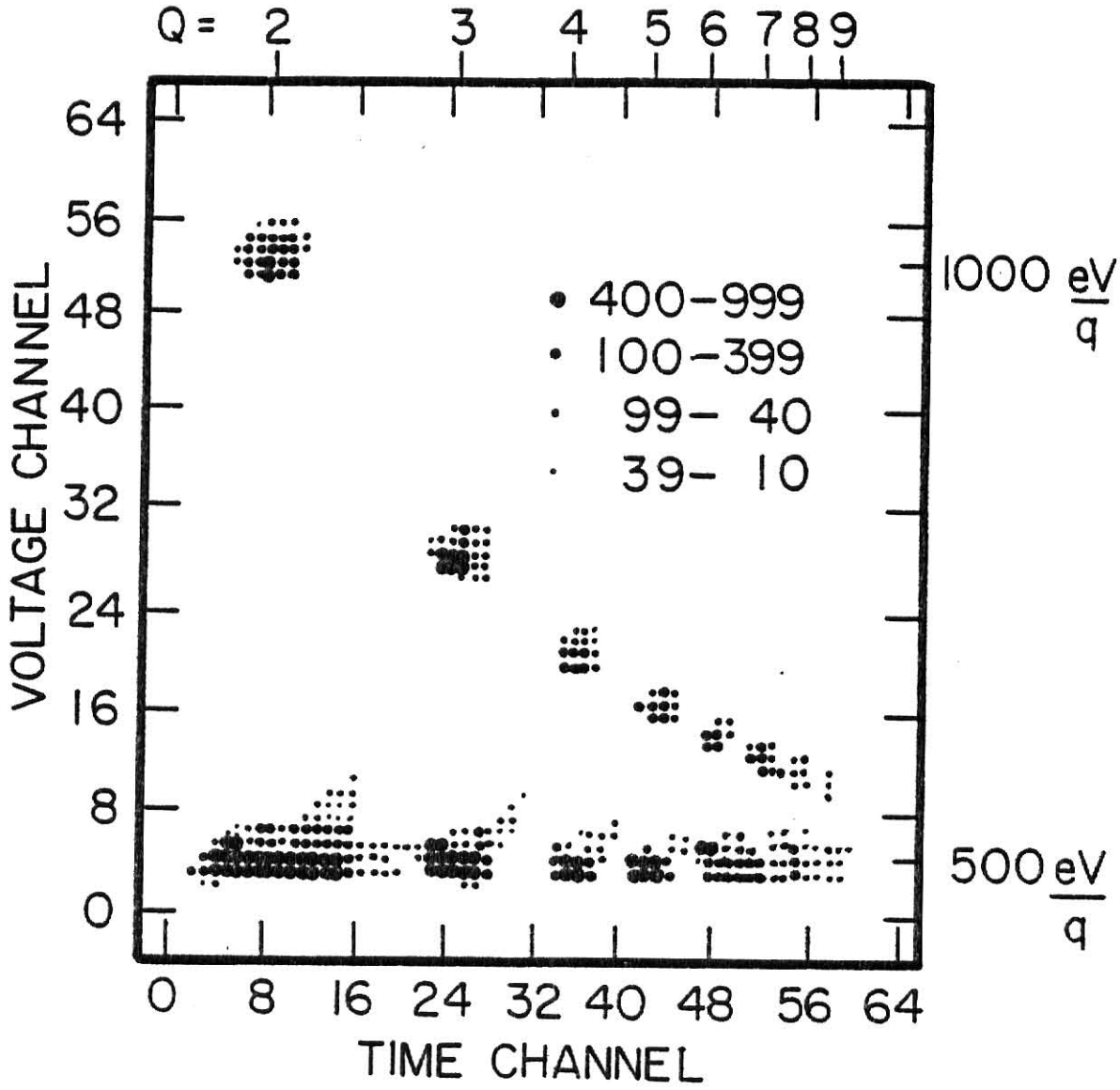
Q = 2 3 4 5 6 7 8 9
64
56
48
40
32
24
16
8
0
VOLTAGE CHANNEL
• 400-999
• 100-399
• 99- 40
• 39- 10
1000 eV/q
500 eV/q
0 8 16 24 32 40 48 56 64
TIME CHANNEL

FIGURE 2

Figure 3: Electronics block diagram for data acquisition.

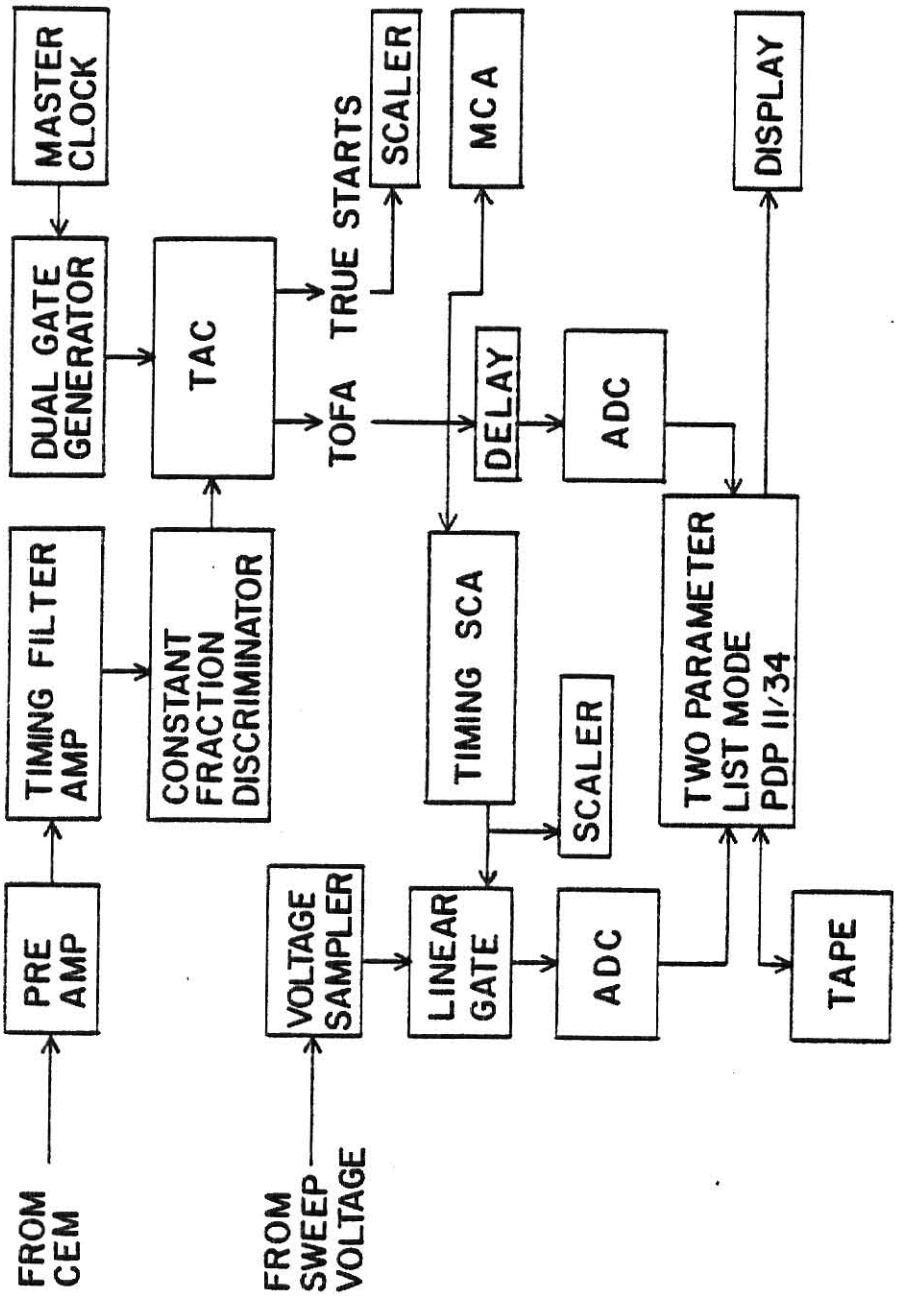
MASTER CLOCK
DUAL GATE GENERATOR
TAC
TRUE STARTS
SCALER
MCA
DISPLAY
TOFA
DELAY
ADC
TIMING FILTER AMP
CONSTANT FRACTION DISCRIMINATOR
TIMING SCA
TWO PARAMETER LIST MODE PDP 11/34
SCALER
PRE AMP
VOLTAGE SAMPLER
LINEAR GATE
ADC
TAPE
FROM CEM
FROM SWEEP VOLTAGE

FIGURE 3

oven. The reference junction of each thermocouple was immersed in an ice bath at 0°C. Tabulated Chrommel-Alumel voltage temperature characteristics were used to determine the temperature of the oven.[10] The Li vapor pressure inside the cell was determined using this temperature and known temperature-pressure relationships.[11] From this pressure the absolute gas target density was then calculated. The oven operated at a temperature near 670°K which corresponds to a pressure of 10^{-7} atm. and a target density of 10^{12} atoms/cm^3.

The most difficult single experimental problem encountered in measuring electron capture cross sections was the determination of the absolute target temperature, and thus density. The difficulty lies in obtaining good thermal contact between the oven walls and the thermocouples. Initially the thermocouples were clamped to the oven by a metal washer held in place by a screw. Later specially designed Omega washer type thermocouples were clamped to the oven. Both arrangements failed to provide adequate thermal contact with the oven. The daily temperature characteristics for a given range of input power applied to the oven were self consistent, but these arrangements failed to provide reproducible results over longer periods of time. Accurate temperature measurement is crucial, since an error in temperature of 15°K results in a target pressure error of a factor of two. Pressure variations as large as a factor of three were seen for a given oven power using these initial arrangements. The final method of mounting the thermocouples directly to the oven by silver soldering them on ensured thermal contact and provided temperature measurements that were reproducible as well as accurate.

One test of our ability to produce accurate and reproducible temperature measurements was to use our apparatus to determine the single electron capture cross section for He^{2+} ions colliding with neutral Li target atoms. Figure 4 shows measured electron capture cross sections,

σ_{2-1}, at different projectile energies for $He^{2+} + Li \rightarrow He^{+} + Li^{+}$ collisions. The open circles represent data collected with the final thermocouple arrangement. The error bars were determined from the reproducibility of the cross section measurements as well as from statistical uncertainties. The data of Murray, et al. and McCullough, et al. are shown also.[12] Although the data sets doe not have overlapping energy ranges there is reasonable agreement between the two sets of data. The consistency of our results with the absolute scale of the work referenced is encouraging, though the cross section versus energy trend differs.

After establishing an absolute target desnity scale we then normalized previous data for which the relative temperature scale was constant. This normalization process consisted of scaling earlier measurements of $Ar^{3+} + Li \rightarrow Ar^{2+} + Li^{+}$ cross sections, Ar σ_{3-2}, to measurements of this cross section made in the final thermocouple arrangement for each particular projectile energy. This represents a temperature scaling, or thermocouple voltage scaling. Figure 5 shows a plot of these corrected thermocouple readings and final set-up thermocouple readings as a function of the power drawn by the oven. As seen in the figure the corrected readings and the actual readings lie along a common power-temperature curve, supporting our interpretation that the source of our absolute scale fluctuations was indeed due to temperature measurement errors.

B. Data Analysis

In order to obtain electron capture cross sections for a projectile ion of charge state q, one first must obtain the normalized yields from the two dimensional spectra. For an event where the initial charge state is q and the final charge state is q' the yield is found by taking a projection on a strip along the time of flight axis in the two dimensional

Figure 4: Single electron capture cross sections for collisions of He^{2+} ions on Li versus center of mass energy of the He^{2+} projectiles. This figure also shows the results of Murray et al. and McCullough, Gilbody et al. (ref. 12).

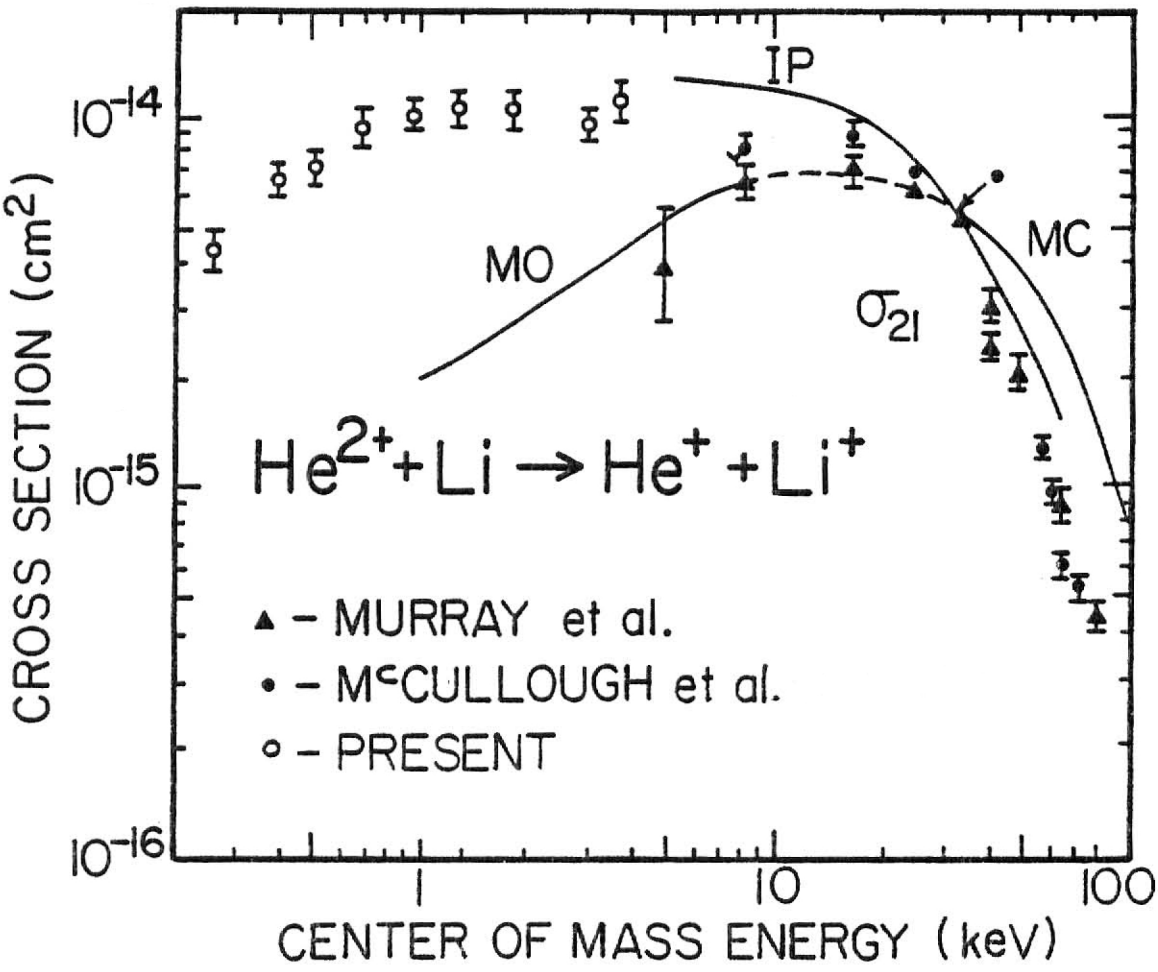
IP
MO
MC
σ_{21}
$He^{2+}+Li \rightarrow He^{+}+Li^{+}$
▲ – MURRAY et al.
• – McCULLOUGH et al.
○ – PRESENT
CROSS SECTION (cm^2)
10^{-14}
10^{-15}
10^{-16}
1
10
100
CENTER OF MASS ENERGY (keV)

FIGURE 4

Figure 5: Applied power required to heat Li vapor oven versus thermocouple voltage.

FIGURE 5

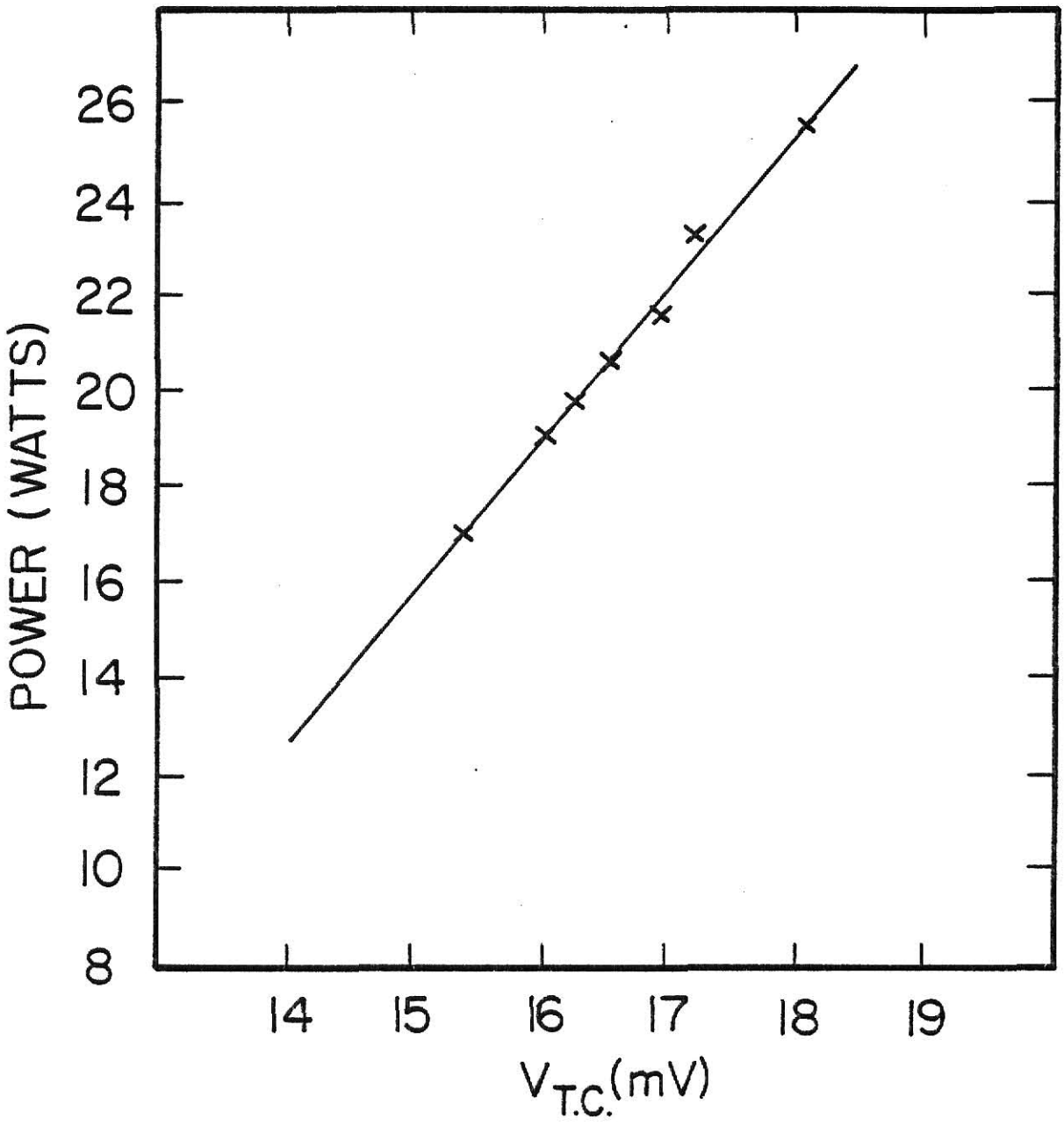

spectra. Projections are chosen for each initial charge state q so as to include all events associated with that charge state. These events are summed over the voltage at which they occurred. A typical projection for q = 5 is shown in Figure 6. Each projection contains a direct peak, where the initial charge state q of the projectile remained unchanged, and peaks associated with the capture of one or more electrons. The normalized yield $Y_{qq'}$ for such an event is given by the following expression:

$$Y_{qq'}(X) = N_{qq'} \frac{q'}{q} \frac{1}{1+(\tau-1)\delta_{qq'}}$$

where

$N_{qq'}$ = Number of background corrected counts in the projection peak associated with projectiles of initial charge state q, and final charge state q'.

τ = Dead time associated with noncapture events.

X = Absolute target thickness in atom/cm^2 = $(n\ell)$

The background correction to the raw number of counts for any case simply entails substracting the random counts contained in the projection peaks, yielding the true number of counts in the peak.

The dead time factor, τ, appears because the rate for direct events is quite large, causing high dead times in the computer which collects the data. These dead times were measured by simultaneously recording the time of flight spectra in a fast pulse height multichannel analyzer which was kept at small, measurable dead times. For an initial charge state q the number of counts stored in the two recording devices were compared allowing a direct calculation of the computer's dead time. Dead times corresponding to charge changing events were neglible due to low counting rates associated with these events.

Figure 6: Projection onto V_A axis of the two-dimensional spectrum for Ar^{5+} on Li.

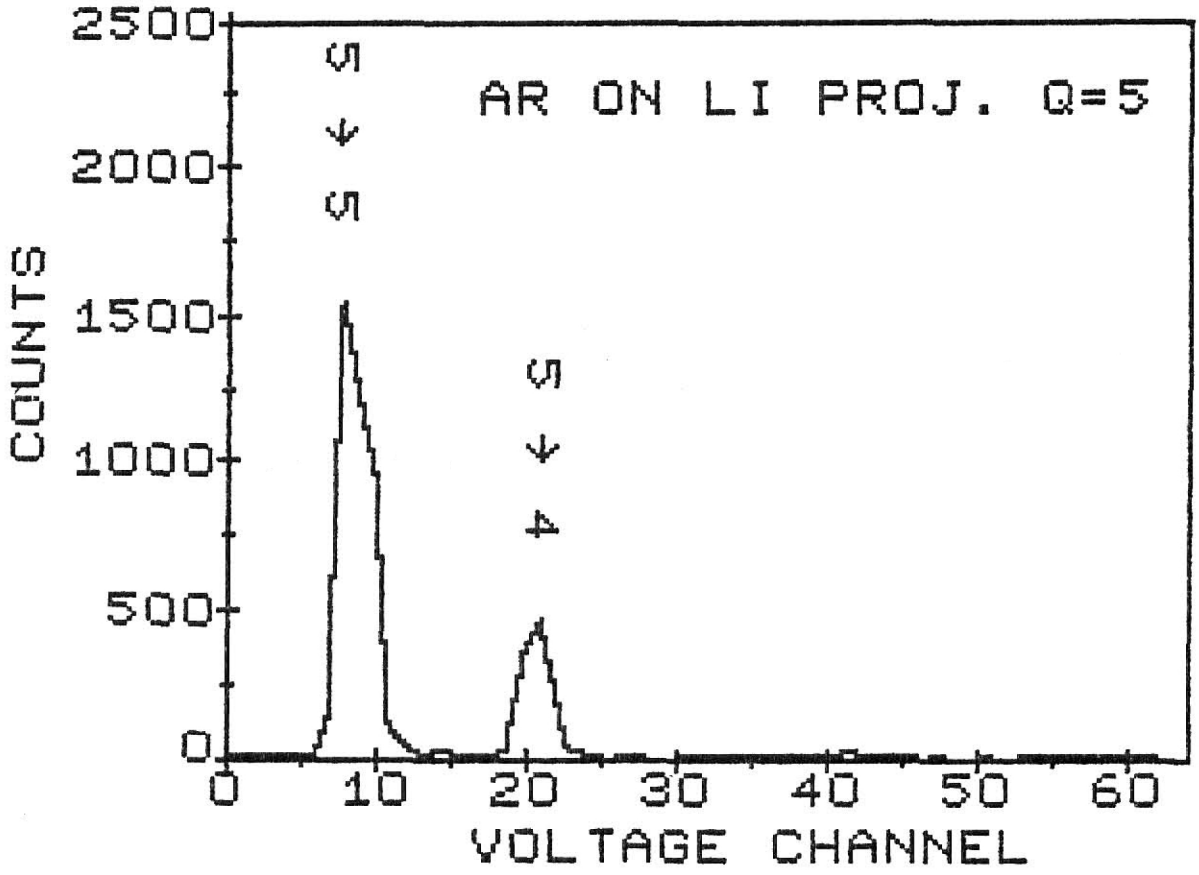
AR ON LI PROJ. Q=5
COUNTS
2500
2000
1500
1000
500
0
0
10
20
30
40
50
60
VOLTAGE CHANNEL

FIGURE 6

Finally, the correction q'/q arises from the finite energy resolution of the analyzer. The time required for the analyzer to sweep through a fixed voltage increment is constant, and thus the time required to sweep through a peak is proportional to the width of the voltage window, δV_A, over which ions are admitted. The analyzer voltage at which a projectile ion passes through the analyzer is proportional to the ratio between the projectile's energy, $q\ V_1$, and charge state q', or

$$V_A = K \frac{qV_1}{q'} \quad .$$

The voltage window δV_A is proportional to V_A with a proportionality constant which depends on the geometry of the analyzer and exit slit. Since V_A is larger for a charge changing event than for a direct event by the factor q/q', the δV_A window for the charge changing event is also larger by this same factor and thus the time spent counting the charge changing events is longer by the factor q/q'. The correction factor q'/q corrects for the longer counting time of charge state changing events.

The absolute target thickness, X, (in atoms/cm^2) was determined from the measured value of the oven path length, and the Li gas density. At all times the oven was operated at temperatures sufficiently low to provide target densities where multiple collision events were negligible.

Cross sections for single electron capture were calculated for incident projectile ions R^{+q} (R = He, Ne, Ar, Kr, Xe) in the manner discussed extensively by Justiniano.[13] This method first calculates a first order cross section by the following expression:

$$\sigma_{q,q-1} = \frac{\dfrac{Y_{q\,q-1}(X)}{Y^{T}_{q}(X)} - \dfrac{Y_{q\,q-1}(X')}{Y^{T}_{q\,q-1}(X')}}{\Delta X} \qquad (1)$$

where the total yield for charge state q is defined as

$$Y^{T}_{q}(X) = \sum_{q'} Y_{qq'}(X) \qquad (2)$$

and $\Delta X = X - X'$.

A small correction is then made by iteratively correcting this cross section for multiple collision events.[13]

The uncertainties present in these cross section measurements are of two types: (1) relative uncertainty, and (2) absolute or systematic uncertainty. The relative uncertainty in a cross section measurement is the reproducibility of that measurement. This uncertainty was used to determine most of the error bars shown in the figures presented in this work. For some cases where a sufficient number of separate runs were not made, the error bars reflect the counting statistics. The ability to measure the target path length, and to determine an absolute target density determines the overall systematic uncertainty. The problems involved with determining an absolute thermocouple temperature - Li target density scale are undergoing further study. The consistency of the measured electron capture cross sections for He^{2+} on Li and those of Murray et al. and McCullough et al.[14] shown in Figure 4 reflect the present systematic uncertainty. Based on this agreement and the systematic uncertainty of 20% reported by these authors, we have assigned an overall systematic uncertainty of 50% to the cross sections presented in this work.

Chapter 3

RESULTS

Measured electron capture cross sections σ_{3-2} for Ar projectiles are presented as a function of Li target density in Figure 7. The deduced cross sections, collected at projectile energies of 500 eV/q, show no systematic dependence on target density. This shows our ability to control relative oven temperatures and consequently target thickness, as well as our ability to produce single collision conditions.

The energy dependence of total electron capture cross sections for collisions involving Li target atoms and Ar, and Ne projectiles are presented in Figures 8 and 9 respectively. Except for the case of Ne projectiles of charge state q = 2, both Ne and Ar cross sections show no dependence on (E/q). Similar results have been reported by Justiniano[15] for collisions between these projectiles and He atoms with the same exceptions occurring for low (q = 2,3) projectile charge states. Figure 10 shows the energy dependence of the total electron capture cross section for Ne q = 2 projectiles. Also presented in this figure are the results of Rille and Winter[16] taken at substantially higher energies. These results, when compared with the experimental values presented here, show a smooth energy dependence in the Ne σ_{2-1} cross section. It was hoped that this reaction could be used to check the temperature scale used to calculate cross sections, but the steep energy dependence of the cross section preclude any such check, since the energy ranges of the two sets of data are far apart.

Figure 7: Single electron capture cross section for Ar^{3+} on Li collisions versus Li target density, n.

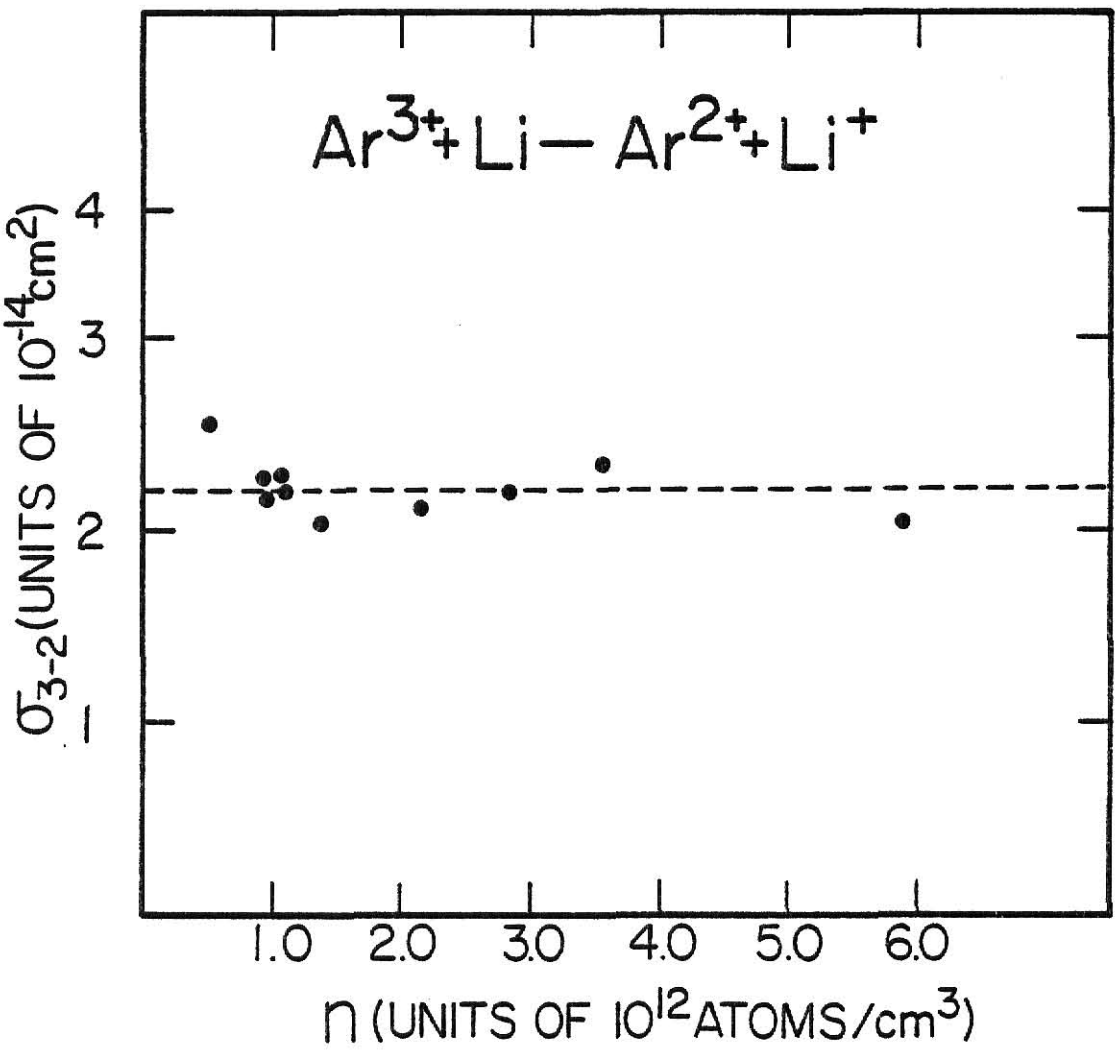
$Ar^{3+} + Li \rightarrow Ar^{2+} + Li^{+}$
σ_{3-2} (UNITS OF $10^{-14} cm^2$)
1
2
3
4
1.0
2.0
3.0
4.0
5.0
6.0
n (UNITS OF 10^{12} ATOMS/cm^3)

FIGURE 7

Figure 8: Electron capture cross sections for collisions of Ar^{q+} on Li versus the energy per charge state of the LEHQ projectile.

FIGURE 8

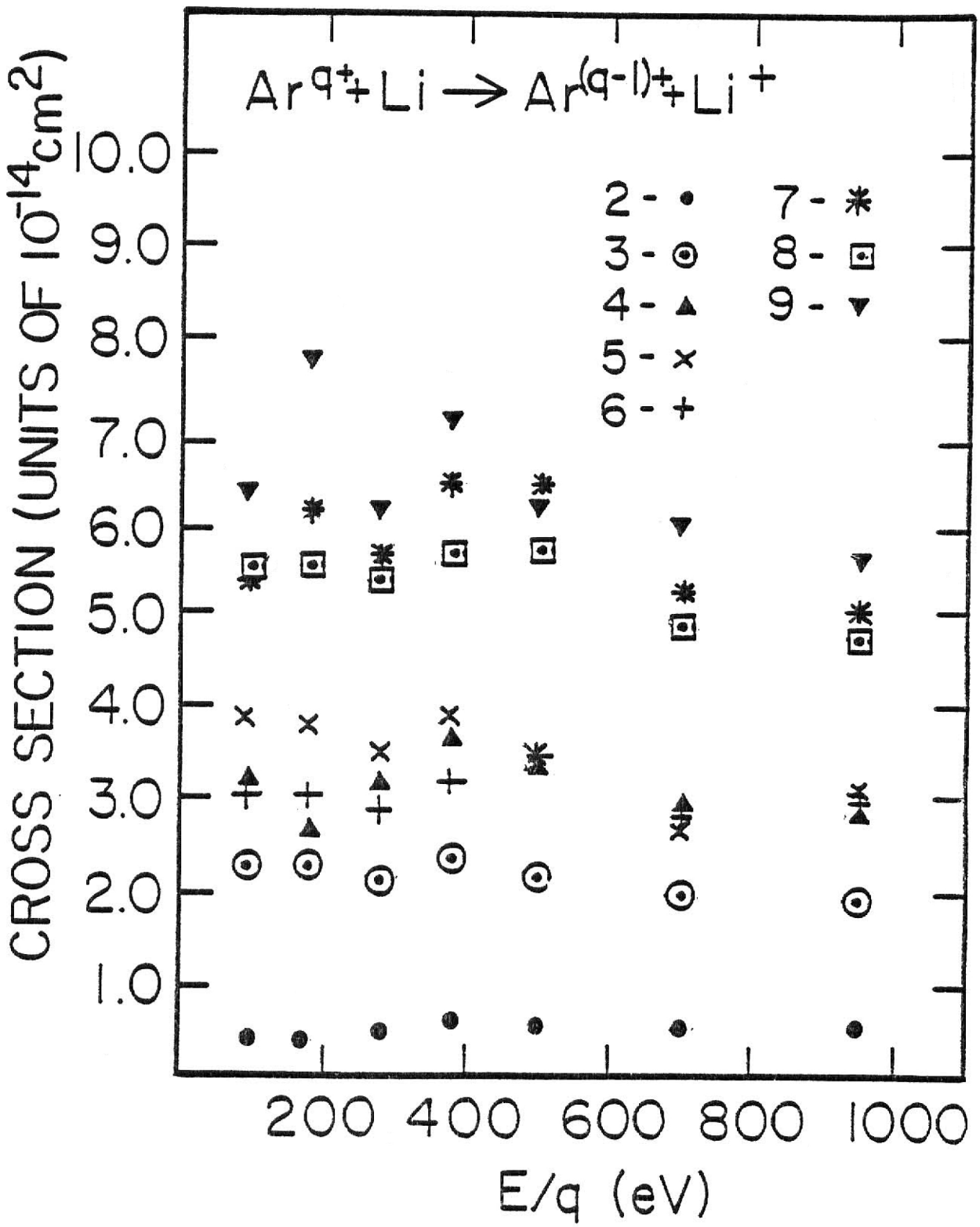
$Ar^{q+} + Li \rightarrow Ar^{(q-1)+} + Li^+$
2 - •
3 - ⊙
4 - ▲
5 - ×
6 - +
7 - ✱
8 - ⊡
9 - ▼
CROSS SECTION (UNITS OF $10^{-14} cm^2$)
10.0
9.0
8.0
7.0
6.0
5.0
4.0
3.0
2.0
1.0
200
400
600
800
1000
E/q (eV)

Figure 9: Electron capture cross sections for collisions of Ne^{q+} on Li versus the energy per charge state of the LEHQ projectile.

FIGURE 9

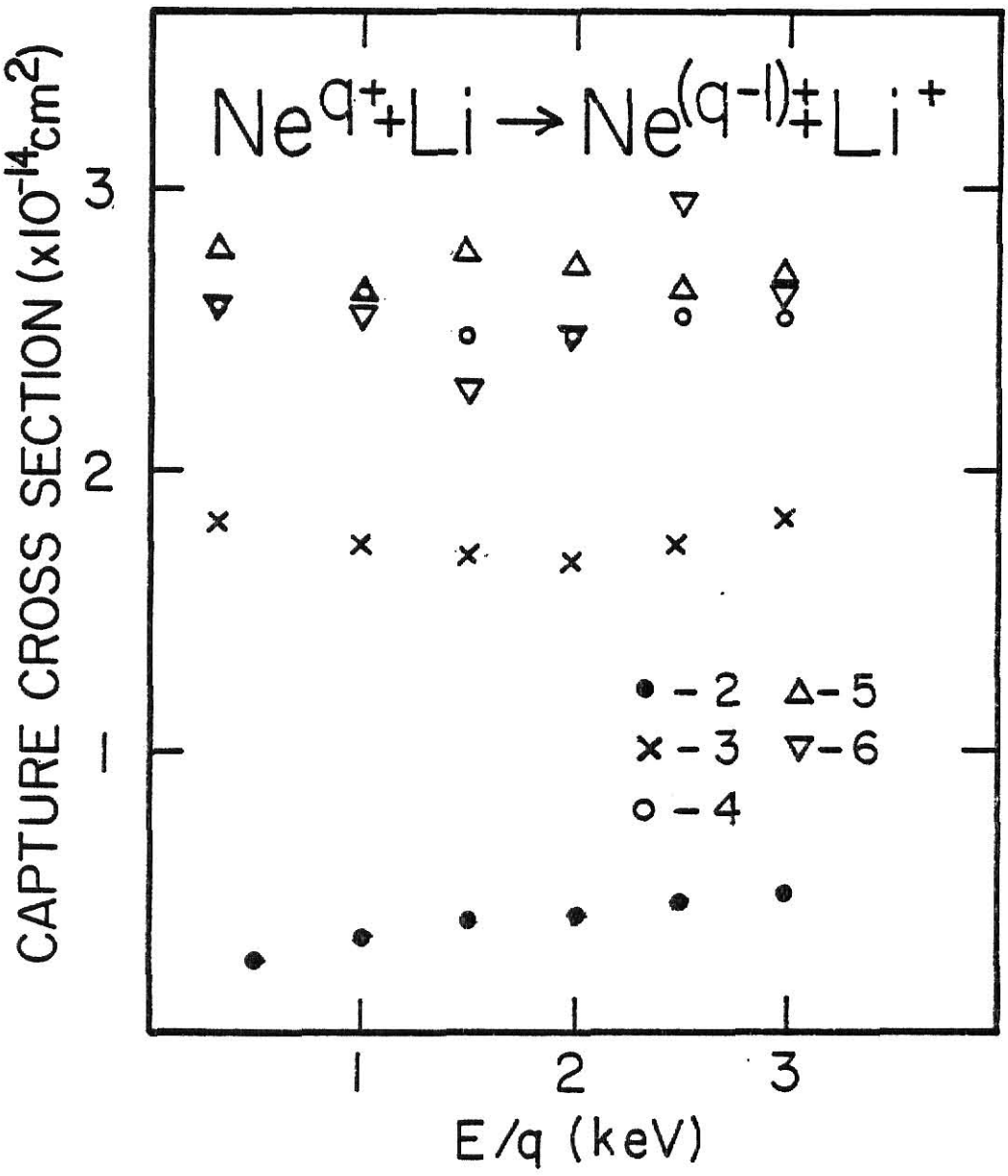
$Ne^{q+}+Li \rightarrow Ne^{(q-1)+}+Li^+$
CAPTURE CROSS SECTION ($\times 10^{-14} cm^2$)
E/q (keV)
1
2
3
● - 2
△ - 5
× - 3
▽ - 6
○ - 4

Figure 10: Single electron capture cross section for Ne^{2+} on Li collisions versus the energy per charge state of the LEHQ projectile.

FIGURE 10

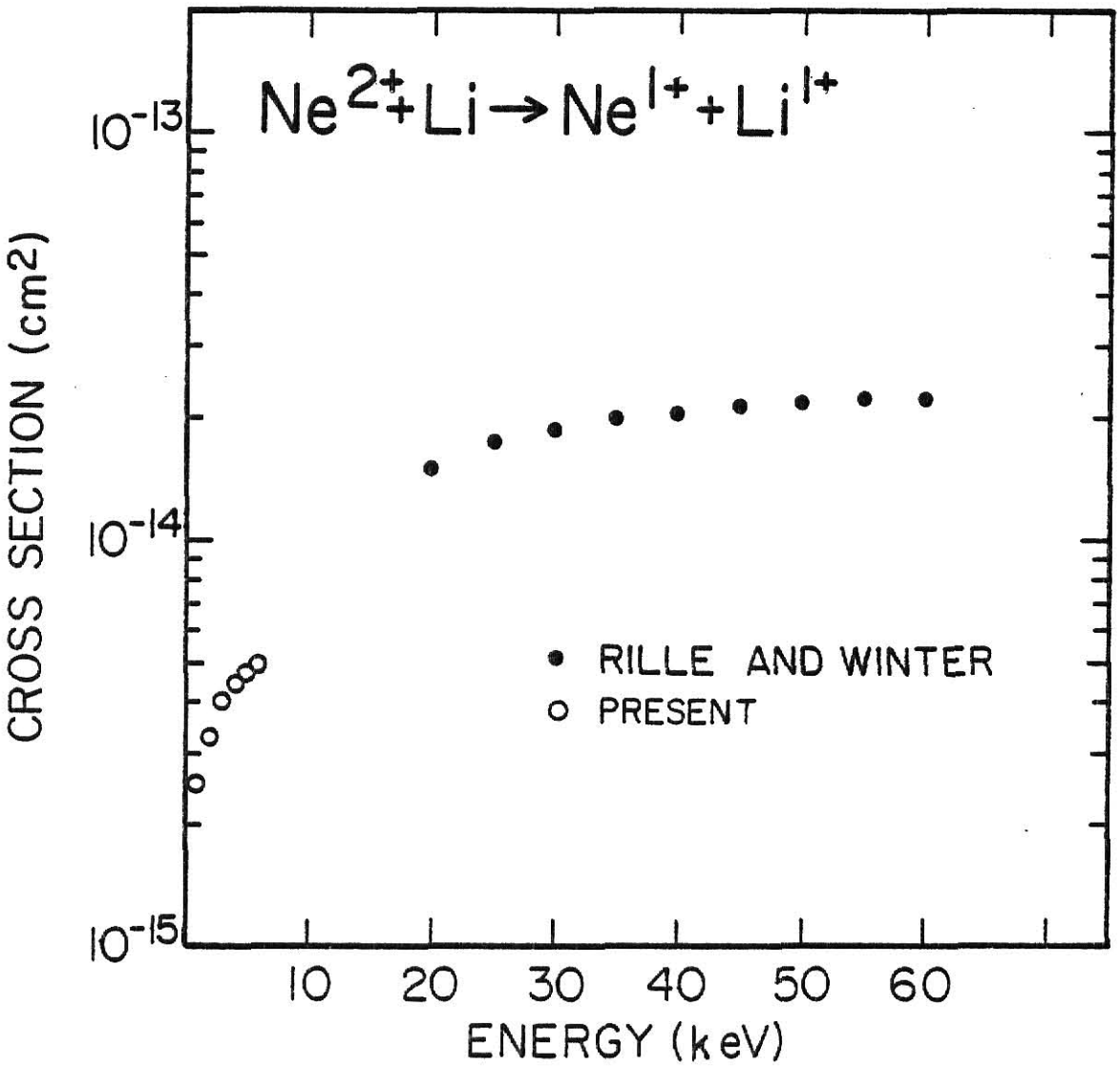
$Ne^{2+} + Li \rightarrow Ne^{1+} + Li^{1+}$
CROSS SECTION (cm2)
10^{-13}
10^{-14}
10^{-15}
10
20
30
40
50
60
ENERGY (keV)
RILLE AND WINTER
PRESENT

The total electron capture cross sections for projectiles R^{q+} (R = Ne, Ar, Kr, and Xe) on Li are presented in Figure 11 as a function of charge state q. The Ar, Kr, and Xe data, as well as the Ne q = 2 data were collected only at a fixed projectile energy per charge of 500 eV/q. For higher Ne charge states some data collected at higher energies were used in the Ne cross section determinations. In all cases the error bars presented represent the scatter in the data collected from a number of independent runs.

The important features evident in Figure 11 are:

(1) The cross sections are nearly independent of projectile species R^{q+} for lower charge states ($2 < q < 7$),

(2) The cross section vary with projectile charge state, ranging from low values for q = 2, 3 to much larger values for q = 8, 9, and a relative maximum value occurs near charge state q = 5. Similar behavior has been reported for these projectiles colliding with He atoms by Justiniano.[17]

Figure 12 presents corrected cross sections for collisions involving R^{q+} projectiles and Li atoms. These cross sections differ from those presented in Figure 12 in that the higher charge states (q = 7, 8, 9) have been corrected for event loss arising from metastable components of the projectile beams. This loss arises because small fractions of the R^{q+} ions are in electronically excited metastable states, such as $(2p^5\ 3s)\ ^3P_{0,2}$ for Ar^{8+} ions. Capture of an electron onto these excited cores forms ions which may autoionize, giving rise to R^{q+} ions which get interpreted as non-capture events. Such events, which appear to be "direct ionization" events, produce an apparent single capture yield which is lower than it should be by this fraction. Such is the case for Ar^{8+} and

Figure 11: Single electron capture cross sections for R^{q+} (R = Ne, Ar, Kr, and Xe) on Li collision versus projectile charge state.

FIGURE 11

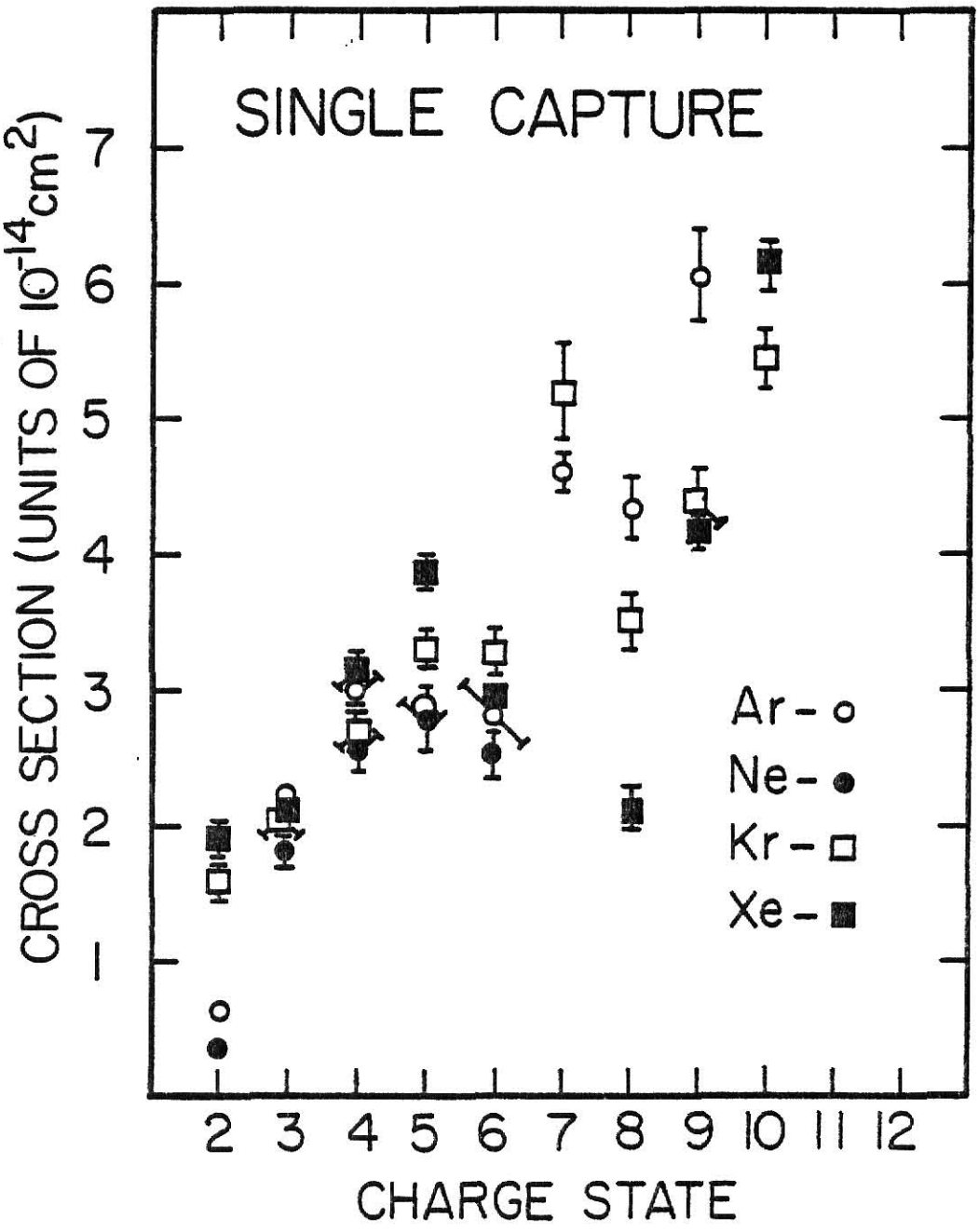
SINGLE CAPTURE
CROSS SECTION (UNITS OF 10^{-14}cm^2)
1
2
3
4
5
6
7
2 3 4 5 6 7 8 9 10 11 12
CHARGE STATE
Ar - ○
Ne - ●
Kr - □
Xe - ■

Figure 12: Corrected capture cross sections for R^{q+} (R = Ne, Ar, Kr, and Xe) on Li collisions versus projectile charge state. Also shown are the Classical Barrier Model, CB, and the Olson and Salop Absorbing Sphere Model, OSAS, calculations.

FIGURE 12

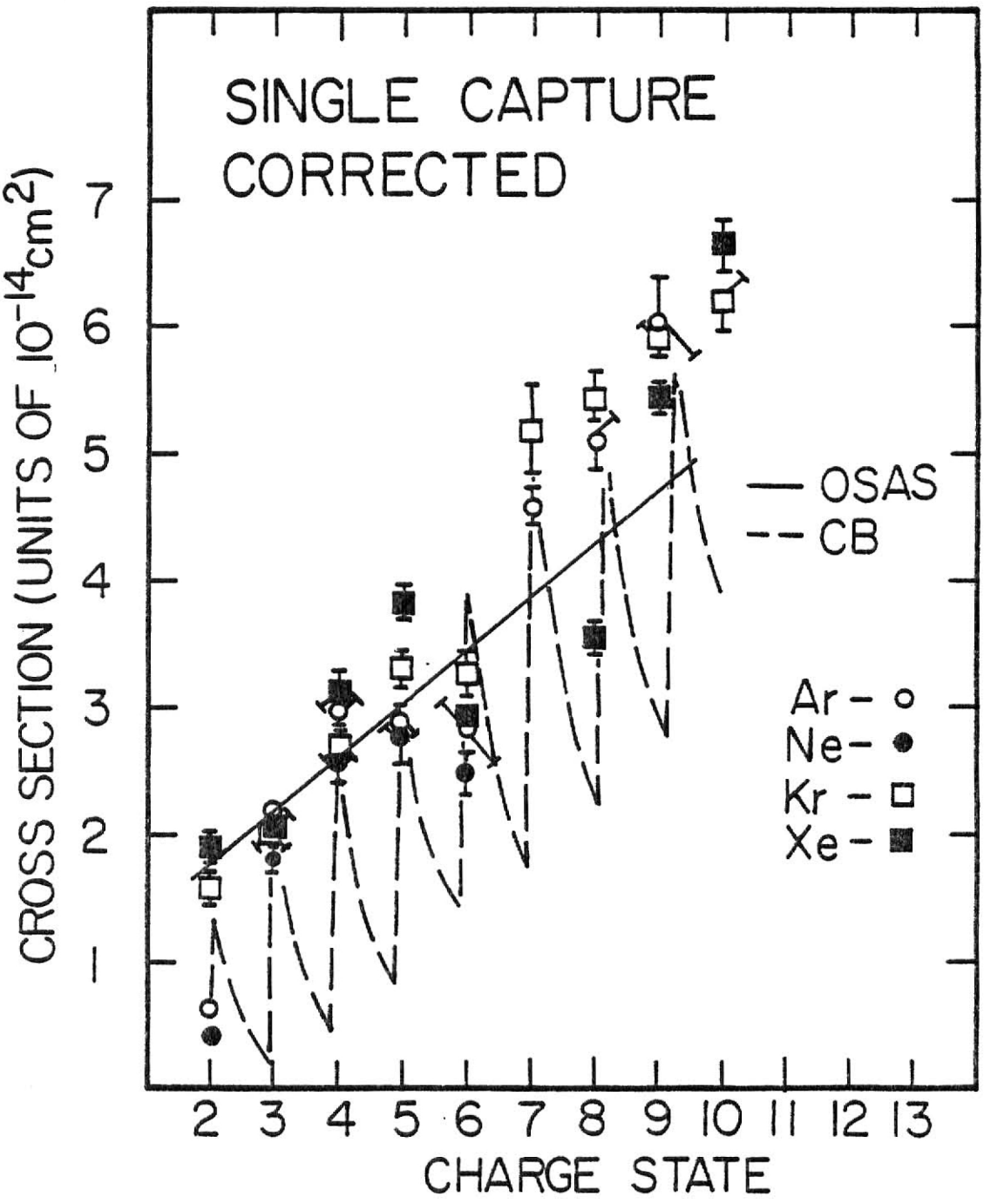
SINGLE CAPTURE
CORRECTED
CROSS SECTION (UNITS OF 10^{-14}cm^2)
1
2
3
4
5
6
7
2 3 4 5 6 7 8 9 10 11 12 13
CHARGE STATE
OSAS
CB
Ar - ○
Ne - ●
Kr - □
Xe - ■

Kr, $(Xe)^{7+, 8+, 9+, 10+}$ ions.

Using a three parameter method which measures projectile initial charge state q, and final charge state q', and the final charge state q" of the targets, Justiniano[17] has measured single capture and so called "direct ionization" cross sections for these R^{q+} ions. The ratio of the direct ionization cross section to the sum of the cross section for single capture and direct ionization measured in this three parameter manner, should be the metastable fraction of the projectile beam. This information was used to correct for event loss in the measured cross sections presented in this work through the following equation:

$$\sigma_{corrected} = \sigma_{measured} \left(1 + \frac{\sigma_{DI}}{\sigma_{SC}}\right)$$

where

$\sigma_{measured}$ ≡ measured cross sections presented in Figure 12

σ_{DI} ≡ Direct ionization cross section for R^{q+} projectiles on He atoms (from previously cited reference[18])

σ_{SC} ≡ Single capture cross sections for R^{q+} projectiles on He atoms (from previously cited reference[18])

The important feature that appears in the corrected cross sections shown in Figure 12 is the independence of cross sections on projectile species R^{q+}, not only for the low projectile charge states, but also for the higher charge states (q = 7,8,9) which contained the metastable components. Also appearing in the figure are the two theoretical curves, OSAS and CB, discussed in Chapter 4. The OSAS model was calculated for incident Ar ions at energies of 500 eV/q. The CB model was calculated using projectile charge q = z.

Chapter 4

THEORY

The theoretical calculations presented here describe the charge transfer of an electron from a neutral atom to a highly ionized low energy projectile. The models presented here have in common the following simplifying assumptions:

(i) The projectile is treated as a structureless charged particle, neglecting the structure of projectile's electronic core. If this treatment is valid, the electron capture cross section will depend only on the charge q of the projectile and not on the projectiles core structure.

(ii) The target atom is treated as a one electron atom.

These assumptions appear particularly well suited for describing rare gas LEHQ projectile ions colliding with neutral Li target atoms. In its ground state configuration, a $1s^2 2s$ state, lithium's loosely bound 2s electron has a binding energy of 5.39 eV. These LEHQ projectiles easily capture this electron. The probability of double electron capture is small, a factor of 10 times smaller than the single capture probability. Furthermore the electron should be captured into Rydberg like states with large n values and at large capture radii. Hence interactions between the electron and the projectiles core charge occur at large distances.

Atomic units will be used throughout this chapter unless otherwise stated.

A. The Classical Model

This model proposed by Ryufuka et al.[18], Mann et al.[19,20], and Beyer et al.[21], assumes that a target electron may be captured in the collision process provided it has enough energy to overcome the potential barrier formed by the coulomb potentials of the projectile and target charge centers. This potential is given by,

$$V(x) = -\frac{z}{x} - \frac{1}{R-x} \tag{3}$$

where x is the distance between the electron and the projectile measured along the internuclear axis. The maximum height of the barrier V_{max} is

$$V_{max} = -\frac{(\sqrt{z}+1)^2}{R} \tag{4}$$

Now the energy of the electron bound to the target in the presence of the projectiles coulomb field is

$$E_{e,t} = -I_t - \frac{z}{R} \tag{5}$$

In order for transfer to occur

$$-I_t - \frac{z}{R} \geq V_{max} \tag{6}$$

or

$$-I_t - \frac{z}{R} \geq -\frac{(\sqrt{z}-1)^2}{R} \tag{7}$$

The electron is captured into a hydrogenlike level of the projectile. The energy of the electron bound to the projectile following capture is determined from the quantum number n of the level into which capture takes place, and from the Coulomb potential of the singly ionized target, and is given by the expression,

$$E_{e,p} = \frac{-z^2}{2n^2} - \frac{1}{R} \tag{8}$$

The radius at which the electron is transferred is given by the crossing of the two potential curves defined in equations (5) and (8), and can be calculated by solving the following expression for R

$$-I_t - \frac{z}{R} = \frac{-z^2}{2n^2} - \frac{1}{R} . \tag{9}$$

A critical, but nonintegral, n_c which just satisfies the transfer conditions given in equations (7) and (9) is found by making eq. (7) an equality and eliminating R from these equations, and is defined by

$$n_c = \left[\frac{z^2}{2I_t}\left(\frac{2\sqrt{z}+1}{z+2\sqrt{z}}\right)\right]^{1/2} \tag{10}$$

The n_c value calculated in this manner is generally not an integrer, but the capture should proceed to a Rydberg state with the nearest integer n smaller than n_c. Using equation (9) to solve for the radius at which this capture occurs, this radius $\bar{R}_x$ is given in terms of n by

$$\bar{R}_x = \frac{2(z-1)}{\frac{z^2}{n^2} - 2I_t} \tag{11}$$

Assuming the probability for electron capture is 1/2, the capture cross section is

$$\sigma_{CB} = \frac{\pi}{2}\bar{R}_x^2 \tag{12}$$

This model predicts cross sections that are independent of the projectile velocity, but dependent on the projectile change state z. The model contains an inherent oscillatory dependence of the cross sections

on charge state, since once an energy level n is reached the critical radius shows an approximate z^{-1} dependence until a new n is allowed. At that point $\overline{R}_x$ increases dramatically.

B. Olson and Salop Absorbing Sphere Model

The description of this model presented here is not intended to be complete, but to serve as an overview of the assumptions inherent in the model, and to provide a comparison to the classical model. For a detailed treatment of the Olson, Salop Absorbing Sphere Model (OSAS) the reader is referred to the literature.[22,23,24,25]

Proposed by Olson and Salop, this model is based on the picture that the capture process takes place through couplings between the entrance molecular orbital (MO) of the neutral target and charged projectile, and the MO's of the final state of the ionized target and projectile. The model assumes that if a large number of exit channels crossing the entrance channel at large internuclear distances are present, then the probability for electron capture can be approximated on the basis of an absorbing sphere.[26] This probability then can be approximated to unity within some critical radius R_c. The cross section for electron capture becomes

$$\sigma_{AS} = \pi R_c^2 \tag{13}$$

where R_c can be determined from the following formula[27]

$$R_c^2 \exp\left(-2.648\ \alpha \frac{R_c}{\sqrt{q}}\right) = 2.864 \times 10^4\ q(q-1)\ V_o\ . \tag{14}$$

Here V_o is the incident projectile velocity, and α is determined by the ionization potential of the target,

$$\alpha = \sqrt{2I_t} \tag{15}$$

Equation (18) can then be solved iteratively to determine the critical radius R_c, and one can then calculate the cross section from this R_c. Unlike the classical model, this model exhibits a slight velocity dependent cross section which increases smoothly as a function of charge state.

Chapter 5

DISCUSSION OF RESULTS

The independence of electron capture cross sections of the energy of the incident projectile has been shown in Figure 8 and Figure 9 for Ar^{8+} and Ne^{q+} projectiles colliding with Li atoms. The lack of energy dependence exhibited in these curves can be atrributed to the large number of exoergic states into which the loosely bound Li target electron can be captured. If the number of exoergic states were small a given reaction channel might dominate the capture process, and as a result any characteristic velocity dependence associated with the probability of the reaction proceeding through this channel would appear in the capture cross section. Figures 13-18 show the energy level diagrams (energy levels vs. internuclear separation) for the $R^{2+} + Li \rightarrow R^{1+} + Li^{+}$ reactions presented here. As seen in these figures, the smallest number of available reaction channels exist for the case of Ne projectiles, thus the Ne σ_{2-1} cross section is most likely to show a velocity dependence, and it does. Since the number of available reaction channels increases with increasing projectile charge state, this velocity dependence is absent for charge states of $q > 2$.

Figure 12 shows the corrected cross sections for rare gas projectile ions on Li atoms as a function of projectile charge state q, in comparison with the theoretical predictions of the OSAS and CB models. Both models predict cross sections that are indpendent of projectile species R^{q+}, and the experimental values exhibit this feature with the possible exceptions being charge states $q = 2$, for Ne and Ar, and $q = 8$ for Xe. In the first

Figure 13: Partial energy-level diagrams for Ne^{2+} on Li. All levels were obtained from tables of references 28 and 29.

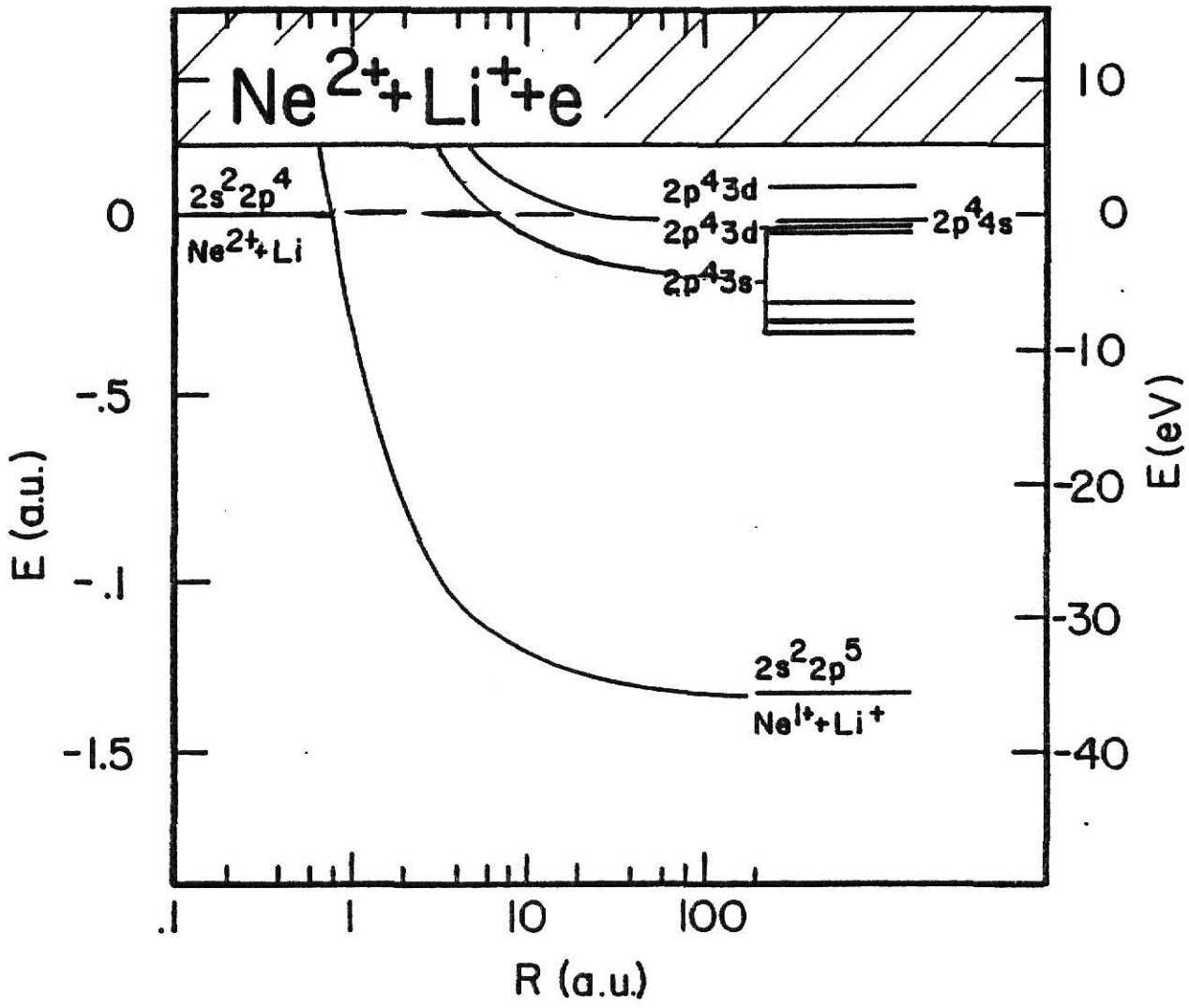
$Ne^{2+}+Li^{+}+e$
$2s^2 2p^4$
$Ne^{2+}+Li$
$2p^4 3d$
$2p^4 3d$
$2p^4 3s$
$2p^4 4s$
$2s^2 2p^5$
$Ne^{1+}+Li^{+}$
E (a.u.)
0
-.5
-.1
-1.5
E(eV)
10
0
-10
-20
-30
-40
.1
1
10
100
R (a.u.)

FIGURE 13

Figure 14: Partial energy-level diagrams for Ar^{2+} on Li. All levels were obtained from tables of reference 28 and 29.

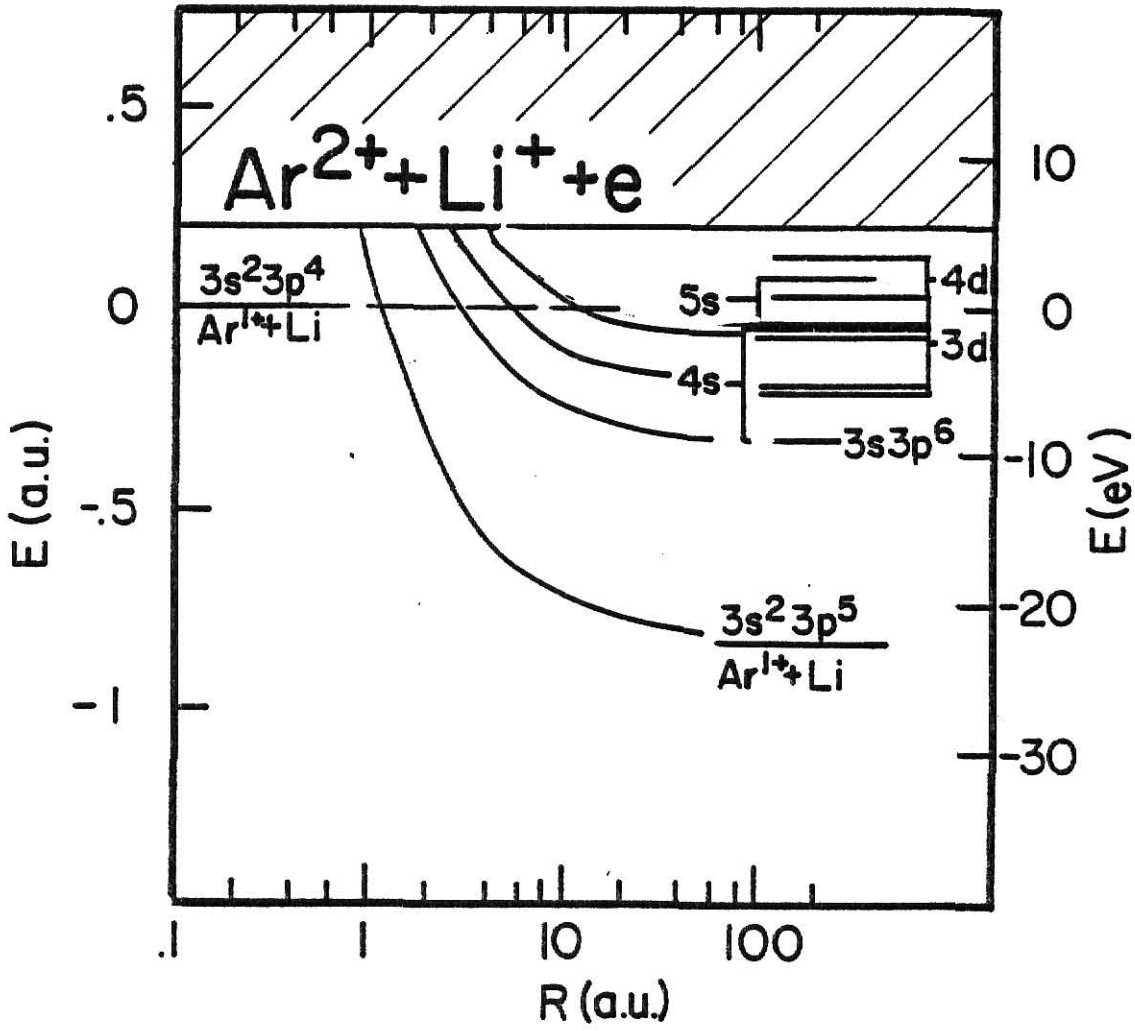
$Ar^{2+}+Li^{+}+e$
$3s^23p^4$
$Ar^{1+}+Li$
5s
4d
3d
4s
$3s3p^6$
$3s^23p^5$
$Ar^{1+}+Li$
.5
0
-.5
-1
10
0
-10
-20
-30
E (a.u.)
E(eV)
.1
1
10
100
R (a.u.)

FIGURE 14

Figure 15: Partial energy-level diagrams for Kr^{2+} on Li. All levels were obtained from tables of reference 28 and 29.

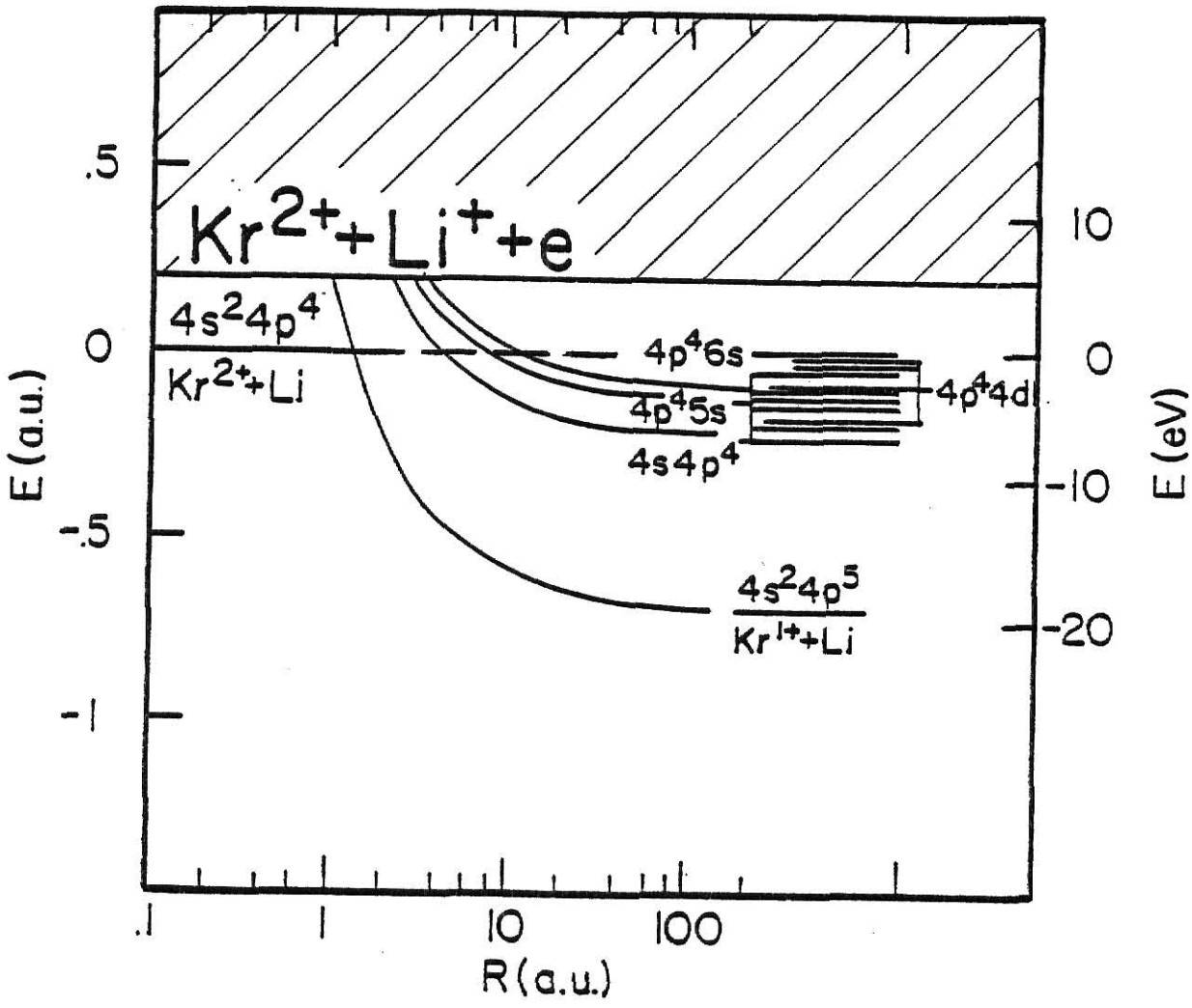
$Kr^{2+}+Li^{+}+e$
$4s^24p^4$
$Kr^{2+}+Li$
$4p^46s$
$4p^45s$
$4s4p^4$
$4p^44d$
$4s^24p^5$
$Kr^{1+}+Li$
.5
0
-.5
-1
E(a.u.)
10
0
-10
-20
E(eV)
.1
1
10
100
R(a.u.)

FIGURE 15

Figure 16: Partial energy-level diagrams for Xe^{2+} on Li. All levels were obtained from tables of reference 28 and 29.

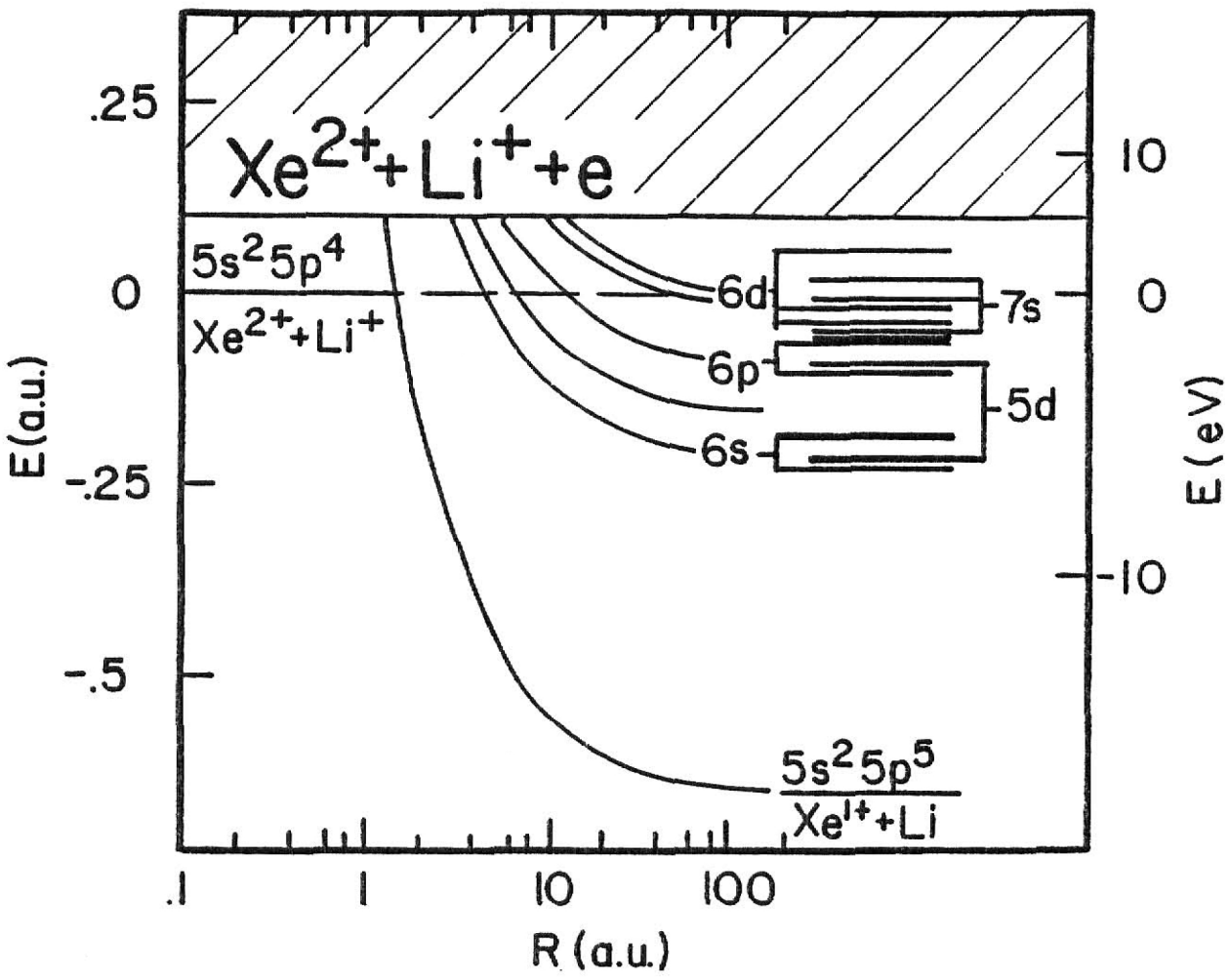
.25
0
-.25
-.5
E(a.u.)
$Xe^{2+}+Li^{+}+e$
$5s^25p^4$
$Xe^{2+}+Li^{+}$
6d
7s
6p
5d
6s
$5s^25p^5$
$Xe^{1+}+Li$
10
0
-10
E(eV)
.1
1
10
100
R(a.u.)

FIGURE 16

Figure 17: Partial energy-level diagrams for Ar^{6+} on Li. All levels were obtained from tables of references 28 and 29.

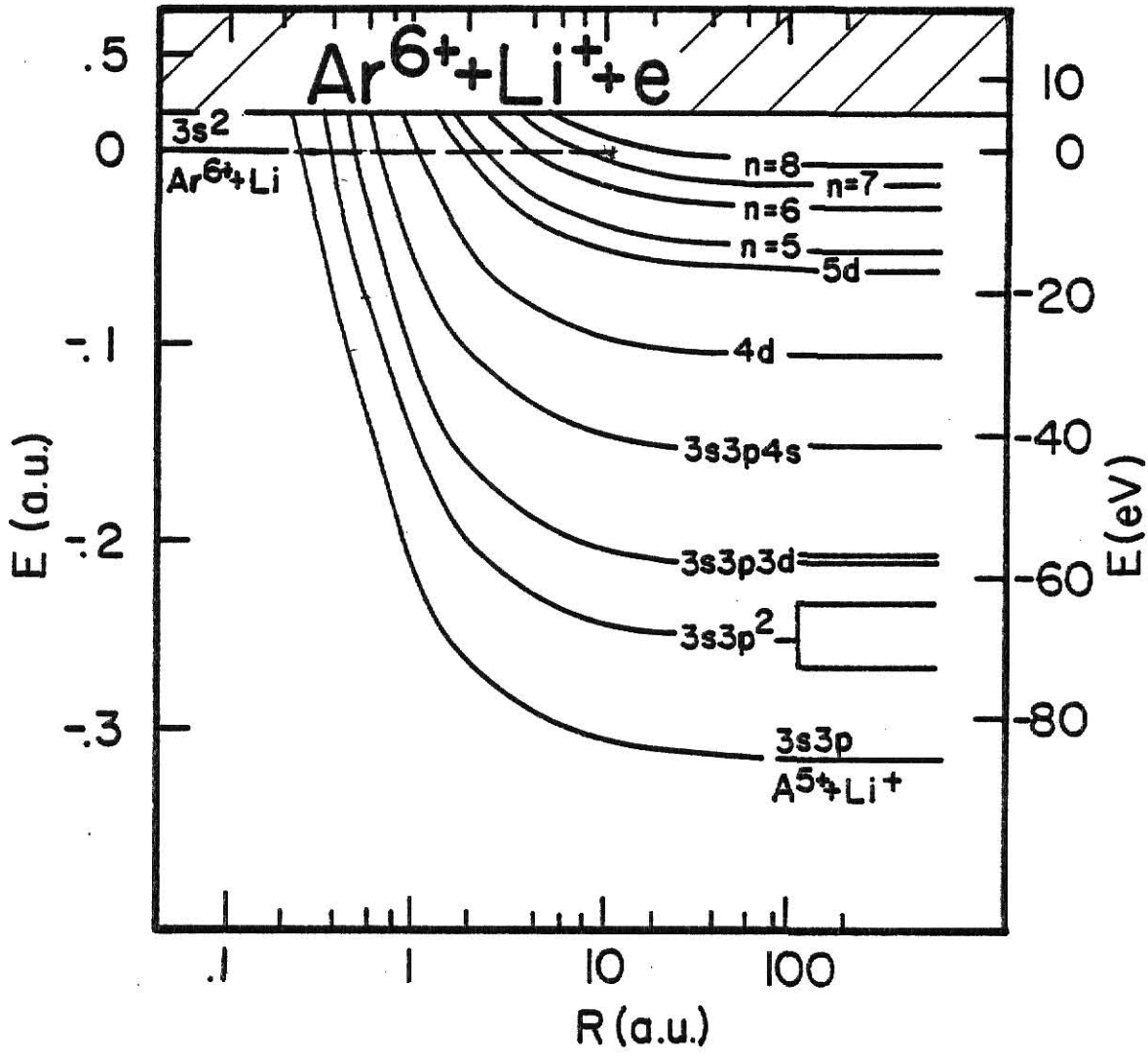
$Ar^{6+}+Li^{+}+e$
$3s^2$
$Ar^{6+}+Li$
n=8
n=7
n=6
n=5
5d
4d
3s3p4s
3s3p3d
$3s3p^2$
3s3p
$A^{5+}+Li^{+}$
.5
0
-.1
-.2
-.3
E (a.u.)
10
0
-20
-40
-60
-80
E(eV)
.1
1
10
100
R (a.u.)

FIGURE 17

Figure 18: Partial energy-level diagrams for Ne^{6+} on Li. All levels were obtained from tables of references 28 and 29.

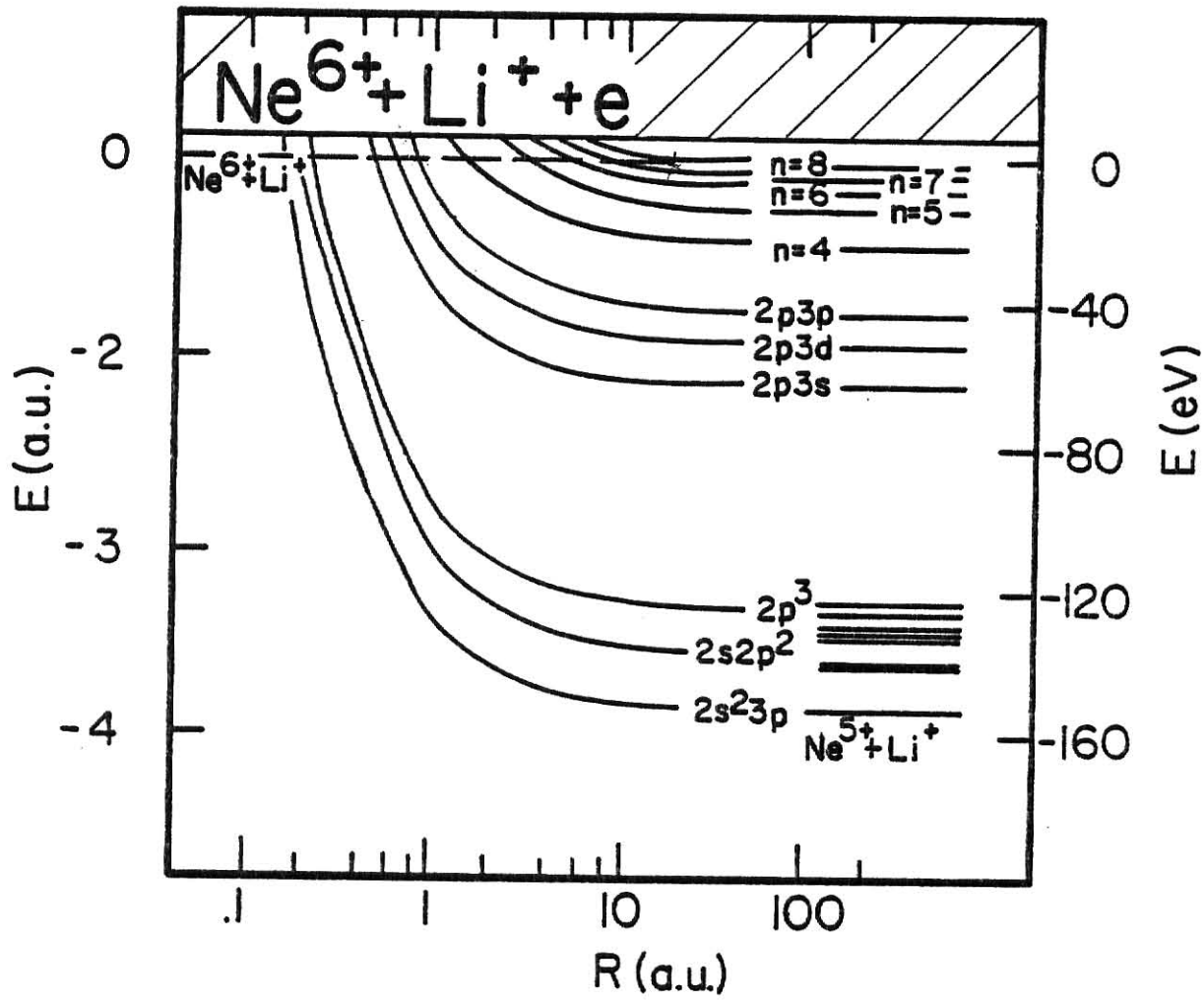
Ne6++Li+ +e
Ne6++Li+
n=8
n=7
n=6
n=5
n=4
2p3p
2p3d
2p3s
2p3
2s2p2
2s23p
Ne5++Li+
0
-2
-3
-4
E(a.u.)
0
-40
-80
-120
-160
E(eV)
.1
1
10
100
R (a.u.)

FIGURE 18

case, the Ar and Ne σ_{2-1} cross sections are about a factor of two lower than the σ_{2-1} cross section of Kr and Xe. This is attributed to the smaller number of exoergic states available in the capture process for Ar and Ne projectiles than Kr and Xe as seen in the energy level diagrams of Figure 13-18. In the other cases, the Xe^{8+} cross section is significantly lower than the Ar^{8+} and Kr^{8+} cross section. This behavior is not presently understood.

The cross sections predicted by the two models presented are in reasonable agreement with the experimental values, especially for the intermediate charge states (q = 3,4,5,6).

The OSAS model predicts cross sections lower than the experimental values for the higher charge states, but is in somewhat better agreement than the CB model. Use of the OSAS model, which is based on a large number of reaction channels might be justified for these high charge states.

Overall, both models provide cross sections reasonably close to the experimental values for these R^{q+} + Li collisions. This is in contrast to the case of R^{q+} + He studied by Justiniano.[27] Thus it appears that the simplifying assumptions of these two theories are met better for R^{q+} + Li collisions than for R^{q+} + He.

Chapter 6

SUMMARY

This work presents the measured electron capture cross sections for collisions involving low energy highly charged (LEHQ) rare gas (Ne, Ar, Kr, and Xe) projectiles with neutral Li atoms. The projectile velocities were low (10^{-6} - 10^{-7} cm/s) compared to the velocities of the target electron. Fast pulsed heavy ion beams produced by a Tandem Van de Graaff accelerator were used to produce the source of LEHQ projectiles. A resistively heated oven was used to produce the Li gas target.

Simultaneous measurement of the initial and final charge states of the LEHQ ions during collisions with Li atoms, as well as the Li target thickness, enableed the electron capture cross section to be determined. The capture cross sections were dominated by capture of a single electron, double capture events being a factor of 10 less probable. Measurement of absolute target thickness proved to be the major experimental problem. Consequently, the electron capture cross sections for He^{2+} projectiles colliding with Li atoms were measured and compared with similar measurements of Murray et al. and McCullought et al. in Figure 4. Although these data sets vary slightly in rage of projectile energies from the work presented here, the absolute cross section scales are in good agreement.

The measured electron capture cross sections of Ne, and Ar were found to be independent of projectile energy, except for the case of Ne^{2+} projectiles. This exception was attributed to the smaller number of available exoergic reaction channels for Ne^{2+} based on arguments using atomic

energy level diagrams.

The measured electron capture cross sections for Ne, Ar, Kr and Xe were corrected for event losses which occurred during data collection as a result of metastable components existing in the higher charge state ion beams (q = 7,8,9,10). These corrected capture cross sections were compared to two theoretical models, the OSAS and CB models. Both models successfully predict the cross sections for intermediate charge states (q = 3,4,5,6) but predict cross sections somewhat smaller than those determined at the higher charge states (q = 7,8,9,10), the OSAS calculations being slightly closer to the experimental values.

REFERENCES

1. D. Anderson, J. McCullen, M.O. Scully, and F.F. Seeby, Opt. Commun. 17 227 (1976).

2. M.O. Scully, W.U. Louisell, and W.B. McKnight, Opt. Commun. 9, 246 (1973).

3. A.V. Vinogradov and J.L. Sobelman, Zh. Eksp. Teor. Fiz. 63, 2133 (1972) [Sov. Phys. - JETP 36, 115 (1973)].

4. D.M. Meade, Nucl. Fusion 14, 289 (1974).

5. H. Vermichel and J. Bodhansky, Nucl. Fusion 18, 1467 (1978).

6. G.A. Murray, J. Stone, M. Mayo, and T.J. Morgan, Phys. Rev. A 25, 1805 (1982).

7. C.L. Cocke, Phys. Rev. A 20, 749 (1979).

8. Tom J. Gray, C.L. Cocke and E. Justiniano, Phys. Rev. A 22, 849 (1980).

9. E. Justiniano, Ph.D. Dissertation, (Kansas State University, 1982).

10. Omega Engineering Inc., Temperature Measurement Handbook (1980).

11. T.B. Douglas, L.F. Epstein, J.L. Dever and W.H. Howland, Journal Am. Chem. Soc. 77, 2144 (1955).

12. G.A. Murray, J. Stone, M. Mayo, and T.J. Morgan, Phys. Rev. A 25, 1805 (1982).

13. E. Justiniano, Ph.D. Dissertation, (Kansas State University, 1982).

14. G.A. Murray, T. Stone, M. Mayo and T.J. Morgan, Phys. Rev. A 25, 1805 (1982).

15. E. Justiniano, Ph.D. Dissertation, (Kansas State University, 1982).

16. E. Rille and H. Winter, J. Phys. B: Atomic. Molec. Phys. 15 3489 (1982).

17. E. Justiniano, Ph.D. Dissertation, (Kansas State University, 1982).

18. H. Ryufuku, K. Sasaki, and T. Watanabe, Phys. Rev. A 21, 745 (1980).

19. R. Mann, F. Folkmann, and H.F. Beyer, J. Phys. B: Atom. Molec. Phys. 14, 1161 (1981).

20. R. Mann, H.F. Beyer, and F. Folkmann, Phys. Rev. Lett. 46, 646 (1981).

21. H.F. Beyer, K.-H. Schartner, and F. Folkmann, J. Phys. B: Atom. Molec. Phys. 13, 2459 (1980).

22. R.E. Olson, J. Chem. Phys. 56, 2979 (1972).

23. A. Salop, Phys. Rev. A 13, 1321 (1976).

24. A. Salop and R.E. Olson, Phys. Rev. A 13 1312 (1976).

25. R.E. Olson and A. Salop, Phys. Rev. A 14 579 (1976).

26. R.E. Olson, J. Chem. Phys. 56, 2979 (1972).

27. E. Justiniano, Ph.D. Dissertation, (Kansas State University, 1982).

28. C.E. Moore, Atomic Energy Levels, Natl. Bur. Stand. (U.S.) Circular No. 467 (U.S. GPO, Washington, D.C., 1971).

29. R.L. Kelly and L.J. Palumbo, Atomic and Ionic Emission Lines Below 2000 Angstroms, NRL Report 7599 (U.S. GPO, Washington, D.C., 1973).

EXPERIMENTAL ELECTRON CAPTURE CROSS SECTIONS IN COLLISIONS OF HIGHLY-CHARGED LOW-VELOCITY RARE GAS IONS WITH LITHIUM ATOMS

by

WILLIAM TRACY WAGGONER

B. A., Hastings College, 1980

AN ABSTRACT OF A MASTER'S THESIS

submitted in partial fulfillment of the

requirements for the degree

MASTER OF SCIENCE

Department of Physics

KANSAS STATE UNIVERSITY
Manhattan, Kansas

1983

ABSTRACT

Experimental electron capture cross sections are presented for neon, argon, krypton and xenon ions in collisions on lithium atoms at collision velocities of 10^6 - 10^7 m/s, for a range of projectile charge states q = 2-9. The single electron capture cross sections dominate, double capture events being two orders of magnitude weaker. Except for Ne^{2+}, the cross sections are nearly independent of projectile species, depending only on projectile charge state. The experimental cross sections are compared to the calculated cross sections of the classical barrier and absorbing sphere models. Experimental and calculated values compared favorably in magnitude.